

# Nanoscale

Accepted Manuscript



This is an *Accepted Manuscript*, which has been through the Royal Society of Chemistry peer review process and has been accepted for publication.

*Accepted Manuscripts* are published online shortly after acceptance, before technical editing, formatting and proof reading. Using this free service, authors can make their results available to the community, in citable form, before we publish the edited article. We will replace this *Accepted Manuscript* with the edited and formatted *Advance Article* as soon as it is available.

You can find more information about *Accepted Manuscripts* in the [Information for Authors](#).

Please note that technical editing may introduce minor changes to the text and/or graphics, which may alter content. The journal's standard [Terms & Conditions](#) and the [Ethical guidelines](#) still apply. In no event shall the Royal Society of Chemistry be held responsible for any errors or omissions in this *Accepted Manuscript* or any consequences arising from the use of any information it contains.

## ARTICLE

# Design of efficient dye-sensitized solar cells with patterned ZnO-ZnS core-shell nanowire arrays photoanodes

Cite this: DOI: 10.1039/x0xx00000x

Received 00th January 2012,  
Accepted 00th January 2012

DOI: 10.1039/x0xx00000x

www.rsc.org/

Xiang Chen,<sup>†a</sup> Zhiming Bai,<sup>†a</sup> Xiaoqin Yan,<sup>a</sup> Haoge Yuan,<sup>a</sup> Guangjie Zhang,<sup>a</sup> Pei Lin,<sup>a</sup> Zheng Zhang,<sup>a</sup> Yichong Liu<sup>a</sup> and Yue Zhang<sup>\*ab</sup>

Fabricating photoanodes with high light-harvesting ability, direct electron pathway and few exciton recombination is a key challenge for dye-sensitized solar cells (DSSCs) today. In this paper, large-scale patterned ZnO-ZnS core-shell nanowire arrays (NWAs) are designed and fabricated as photoanodes for the first time. By using the NWAs photoanodes with hexagonal symmetry and FTO-Pt cathodes with Al reflecting layer, the DSSCs demonstrate the highest efficiency of 2.09%, which is improved by 140% compared to the reference cells with line symmetry and without reflecting layer. The improvement is attributed to the enhanced light-harvesting ability of the patterned NWAs, as well as to the remarkable double absorption caused by the Al reflecting layer. Besides, the ZnO core provides direct electron pathway and the ZnS shell reduces exciton recombination simultaneously. This study shows an effective way to improve the performance of DSSCs and could be extended to other nanodevices and nanosystems.

## Introduction

Due to the advantages of inexpensive, color rendition, flexible and biocompatibility, dye-sensitized solar cells (DSSCs) have received considerable interest as one of the most promising devices for converting solar energy to electricity in recent years.<sup>1-4</sup> Mesoporous TiO<sub>2</sub> nanoparticle film has been commonly used in conventional DSSCs due to its sufficient dye adsorption and high conversion efficiency (up to 12.3% by Michael Grätzel).<sup>5,6</sup> However, a further increase in power conversion efficiency ( $\eta$ ) has been limited by energy loss due to recombination occurred on the interfaces (TiO<sub>2</sub>/TiO<sub>2</sub>, FTO/TiO<sub>2</sub> and FTO/electrolyte) during the charge transport process.<sup>7</sup> Such a recombination will become significantly serious when the thickness of the TiO<sub>2</sub> film is increased.<sup>8</sup> Therefore, maximum charge injection and minimum recombination are the key to achieve higher efficiency DSSCs.<sup>2</sup>

ZnO has higher electron mobility (205-1000 cm<sup>2</sup> V<sup>-1</sup>S<sup>-1</sup>) than TiO<sub>2</sub> (0.1-4 cm<sup>2</sup> V<sup>-1</sup>S<sup>-1</sup>).<sup>9</sup> Replacing the TiO<sub>2</sub> nanoparticle film with a array of single-crystalline ZnO nanowire is an effective way to facilitate electron collection, because it can provide higher crystallinity and a direct rather than zigzag pathway for electron transfer.<sup>8,10</sup> However, the efficiency of ZnO-based DSSCs reported so far still remains lower than the DSSCs based on TiO<sub>2</sub>, leaving plenty of room to improve the efficiency through structural and morphology modification of

the electrode.<sup>11</sup> There are two major reasons for that low outcome. One is the recombination of the electrons (injected into the ZnO) with either the dye or the redox electrolyte. The other is chemical instability of ZnO in acid dye, which blocks the electron injection from the dye to ZnO.<sup>11</sup> To overcome these limitations, one of the most promising treatments is adding a thin layer on the ZnO nanowire surface to passivate the recombination sites and increase the chemical stability.<sup>12</sup> ZnS layer is proved to be an effective option as a shell layer on the ZnO nanowire arrays (NWAs) for the application of DSSCs.<sup>13-16</sup> For instance, Lim's group reported that the DSSCs with ZnO-ZnS core-shell NWAs prepared in NH<sub>4</sub>OH (ZTA) solution exhibited a significant increase in cell performance ( $\eta$ =2.72%) compared with the ones without a shell structure ( $\eta$ =0.11%).<sup>13</sup> Besides, Chen's group also found that the performance was significantly improved for the ZnO-ZnS core-shell photoanode fabricated in thiocetamide (TAA) solution ( $\eta$ =1.92%) compared with as-synthesized ZnO photoanode ( $\eta$ =0.12%).<sup>15</sup> To summarize, there are three important functions for the ZnS shell. First of all, ZnS prevents tunneling of the electrons from the ZnO core to the ZnS shell due to a higher band gap of ZnS, so the excited electrons can be confined inside the ZnO.<sup>14</sup> Moreover, the ZnS shell forms a type II band alignment on ZnO core through the induction of charge separation at the interface of the two different materials. Thus

the electrons and holes are localized in different regions and the recombination of the charge carriers can be reduced.<sup>17</sup> In addition, the ZnS shell with coarse surface can enlarge the internal surface area to absorb more dye molecules, resulting in increment of the short-circuit current density ( $J_{sc}$ ).<sup>15</sup>

To further increase solar cell efficiency, one of the most accessible and attainable routes is to modify its optical design to enhance the harvest of total incident light within the cell.<sup>4</sup> That is, maximum light absorption on photoanode and maximum light reflection on cathode are also the key to achieve higher efficiency DSSCs. Many light-harvesting approaches have recently been proposed, such as 3D hierarchical nanostructures,<sup>18-20</sup> photonic crystals,<sup>21,22</sup> plasmonic effects<sup>23-26</sup> and nanopatterned electrode.<sup>27,28</sup> Among them, nanopatterning is a renowned method for constructing photonic nanostructures, and has received tremendous attention as a means of boosting the efficiency in silicon<sup>29-31</sup> and polymer<sup>32,33</sup> solar cells. For DSSCs, Kim's group reported that patterned TiO<sub>2</sub> nanoparticle film gives 40% and 33% enhancement of the  $J_{sc}$  and  $\eta$ .<sup>27</sup> Jung's group found that patterned ZnO hemisphere embedded TiO<sub>2</sub> nanoparticle film demonstrates the highest  $\eta$  of 11.12%, which is improved by 46.5% compared to the reference cell without ZnO hemisphere.<sup>28</sup> Despite all this, facile synthesis of large-scale patterned ZnO-ZnS core-shell NWAs, and their effects on the performance of DSSCs have rarely been reported. Besides, there are few reports focusing on the light management of FTO-Pt cathode, which is commonly used in DSSCs.

Herein, the first large-scale patterned ZnO-ZnS core-shell NWAs were fabricated by using two-beam laser interference lithography (2BLIL), hydrothermal synthesis (HTS) and chemical conversion synthesis (CCS).<sup>34,35,15</sup> 2BLIL is a simple, quick and maskless tool for fabricating large-area, nanometer-scale and periodically patterned structures.<sup>36</sup> Moreover, HTS and CCS are both low temperature techniques with merits of low cost, high yield and easy scale-up.<sup>35,15</sup> We found that the arrangement and density of the patterned ZnO-ZnS core-shell NWAs show remarkable influences on the light absorption of the photoanodes and the performance of the DSSCs. The application of patterned ZnO-ZnS core-shell NWAs with hexagonal symmetry resulted in 60% and 88% enhancement of the  $J_{sc}$  and  $\eta$  compared with the reference cells based on patterned NWAs with line symmetry. Moreover, a FTO-Pt cathode with Al reflecting layer on the back side was employed in this study and played an important role in further increasing the  $J_{sc}$  and  $\eta$ . Overall, enhanced light harvesting on both photoanode and cathode is the key to these gratifying results.

## Experimental

**Chemicals.** AR-N 4340, AR 300-12, AR 300-475 and AR 300-72 (Allresist GmbH); Aquatar (AZ Electronic Materials); Acetone, isopropyl alcohol (IPA), zinc nitrate ( $M=297.49 \text{ g mol}^{-1}$ ) and hexamethylenetetramine (HMTA) ( $M=140.19 \text{ g mol}^{-1}$ ) (Sinopharm Chemical Reagent); Thiacetamide (TAA) ( $M=75.13 \text{ g mol}^{-1}$ ) (Tianjin Kermel Chemical Reagent); N719 dye (DHS-N719,  $M=1187.7 \text{ g mol}^{-1}$ ), Surlyn sealing spacer

(DHS-SN1725, 25  $\mu\text{m}$ ), liquid electrolyte (DHS-E23, redox couple:  $\text{I}^3/\text{I}^-$ , solvent: acetonitrile) (Dalian Heptachroma SolarTech).

**Fabrication of photoresist templates via 2BLIL.** Firstly, AZO-ZnO films (AZO:  $\sim 900 \text{ nm}$ , resistance:  $\leq 10 \Omega \text{ sq}^{-1}$ , transmittance:  $\geq 80\%$ ; ZnO:  $\sim 50 \text{ nm}$ ) were successively deposited on float glass by radio frequency magnetron sputtering (RFMS). As electrode and growing substrate, it was cut into small pieces (15 mm  $\times$  10 mm), ultrasonically cleaned in acetone, IPA and deionized water each for 5 min, and blow-dried using N<sub>2</sub> gas. Secondly, negative photoresist (PR) AR-N 4340 was diluted with thinner AR 300-12 (1:1 weight ratio), and spin-coated on the substrate at 4000 rpm min<sup>-1</sup> for 20 s to form a PR film ( $\sim 400 \text{ nm}$ ), which was followed by a soft baking process at 85 °C on hotplate for 2 min. Aquatar was then spin-coated on the PR film at 3000 rpm min<sup>-1</sup> for 30 s to form a top anti-reflective coating (TARC) ( $\sim 56 \text{ nm}$ ). Thirdly, the PR+TARC coated substrates were exposed by 2BLIL.<sup>34</sup> Herein, four exposure modes and two exposure times (single exposure at 0° for 80 s, double exposure at 0°+30°, 0°+60° and 0°+90° for 35+35 s) were employed. Finally, the substrates were postbaked at 95 °C on hotplate for 80 s, developed in AR 300-475 and deionized water mixed solution (1:1 volume ratio) for 6 min, rinsed with deionized water for 30 s and blow-dried using N<sub>2</sub> gas to obtain four kinds of PR templates (period of 1  $\mu\text{m}$ ) on the substrates (Fig. S1, ESI†). These PR templates (with line, long hexagonal, hexagonal and square symmetries) were applied to define the nucleation sites and arrangements of patterned ZnO-ZnS core-shell NWAs.

**Synthesis of patterned ZnO-ZnS core-shell NWAs via HTS and CCS.** Patterned ZnO NWAs were firstly synthesized in 50 ml aqueous solution of equimolar (0.05 mol L<sup>-1</sup>) zinc nitrate and HMTA, with the templated substrates up-side down at 95 °C for 3 h. After the solution was cooled down, the substrates were taken out and cleaned by rinsing with PR remover AR 300-72 for 30 s, deionized water for 1 min, IPA for 1 min and dried in oven at 60 °C for 10 min. Then, the substrates covered with patterned ZnO NWAs were immersed in TAA aqueous solution (0.2 mol L<sup>-1</sup>) at 90 °C to form the ZnS shell. Noted that the  $J_{sc}$  and  $\eta$  can reach a maximum after 6 h sulfidation time ( $T_s$ ),<sup>15</sup> thus  $T_s$  is fixed at 6 h in this study. At last, the substrates were cleaned with deionized water for 1 min and dried in oven at 60 °C for 30 min.

**Cell fabrication.** For dye adsorption, the patterned ZnO-ZnS core-shell NWAs as photoanodes were immersed in 0.3 mmol L<sup>-1</sup> N719 dye in ethanol solution at 60 °C for 40 min, followed by briefly rinsing with ethanol and drying in air. Pt-coated FTO glass (15 mm  $\times$  10 mm, resistance:  $\leq 10 \Omega \text{ sq}^{-1}$ , Dalian Heptachroma SolarTech) (with or without Al reflecting layer) was used as counter electrode. Two holes (0.75 mm diameters) were pre-drilled in the FTO glass for injecting electrolyte. After that, dye-adsorbed NWAs photoanode and FTO-Pt cathode were stack and sealed with Surlyn sealing spacer at 120 °C for

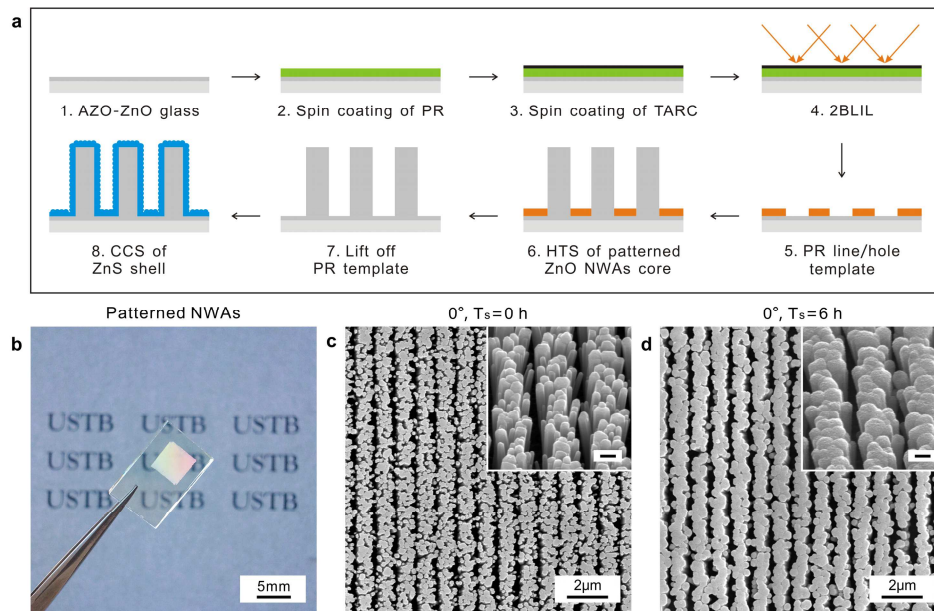


**Fig. 1** (a) Schematic illustration of the fabrication sequence of patterned ZnO-ZnS core-shell NWAs via 2BLIL, HTS and CCS. (b) Optical image of an AZO-ZnO glass covered with patterned ZnO-ZnS core-shell NWAs ( $\sim 0.25 \text{ cm}^2$ ). (c-d) Top view SEM images of the patterned ZnO NWAs (c) and ZnO-ZnS core-shell NWAs (d) with line symmetry. Insets give the corresponding magnified  $45^\circ$  titled view SEM images, scale bars are 300 nm.

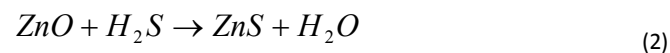
10 s. The effective area of the photoanodes was  $\sim 0.25 \text{ cm}^2$ . Liquid electrolyte was introduced into the sandwich solar cells through the drilled holes. Then the holes were sealed by parafilm at elevated temperature.

**Characterization.** The morphologies of PR templates and patterned ZnO-ZnS core-shell NWAs, and X-ray energy dispersive spectroscopy (EDS) analysis were conducted by field emission scanning electron microscopy (FESEM, FEI QUANTA 3D). The crystal structure and orientation of the NWAs were investigated by X-ray diffraction (XRD, Rigaku DMAX-RB,  $\text{CuK}\alpha$ ). UV-vis absorption of the NWAs photoanodes and reflectance of the FTO-Pt cathodes were carried out using a UV-vis spectrometer (Varian Cary 5000). The current-voltage (J-V) characteristics of the cells were measured by an electrochemical workstation (Solartron SI 1287/SI 1260) under AM 1.5G illumination provided by a solar simulator (Oriel, 91159A,  $100 \text{ mW cm}^{-2}$ ).

## Results and discussion

The fabrication sequence of patterned ZnO-ZnS core-shell NWAs via 2BLIL, HTS and CCS is shown in Fig. 1a. More details are provided in "Experimental" section. Noted that the color of the substrate will be changed in each step, especially when the substrate is covered with patterned NWAs (Fig. 1b). The bright color caused by light diffraction indicates a large-scale patterned ZnO-ZnS core-shell NWAs over the surface, which will benefit the realization of efficient DSSCs. Based on PR line template (Fig. S1a, ESI<sup>†</sup>), patterned ZnO NWAs in a period of  $1 \mu\text{m}$  with line symmetry were fabricated first ( $T_s=0 \text{ h}$ ) (Fig. 1c). It is clear that the ZnO NWAs (diameter:  $\sim 200 \text{ nm}$ ,

length:  $\sim 2.2 \mu\text{m}$ ) are uniformly distributed and vertically aligned on the substrate, and multiple NWAs grow out of each line due to the PR space was so wide that lots of small ZnO grains were exposed.<sup>37</sup> After sulfidation in the TAA solution ( $T_s=6 \text{ h}$ ), many adjacent NWAs stick together and the surface of ZnO NWAs becomes coarse (Fig. 1d). That's because during the sulfidation process, a ZnS shell is fabricated on the ZnO core by the following reactions:<sup>38</sup>



When the solution reaches a certain temperature, TAA is hydrolyzed and releases  $\text{H}_2\text{S}$  due to the reaction (1). Ions exchange between  $\text{H}_2\text{S}$  and ZnO by the reaction (2) occurs as sulfur ions react with zinc ions to form the initial ZnS shell on the ZnO surface. As reaction (2) goes on, the ZnS shell becomes thicker due to more and more ZnS nanoparticles pile up on the initial ZnS shell.<sup>39</sup> However, the growth of ZnS shell will then be limited by the insufficient sulfur source for the low concentration of TAA. Therefore, a thin and porous ZnS shell is fabricated on the patterned ZnO NWAs core at last.<sup>40</sup>

The crystal structure and chemical composition of the NWAs were characterized by XRD and EDS. For  $T_s=0 \text{ h}$ , the XRD pattern shows only two main peaks at  $34.45^\circ$  and  $72.56^\circ$ , corresponding to the ZnO (002) and (004) planes. It indicates that the NWAs consist of pure single-crystalline highly c-axis oriented ZnO (Fig. 2a). For  $T_s=6 \text{ h}$ , the diffraction peak of ZnO is still very strong. However, there is also a weak peak corresponding to the ZnS (111) plane, which is similar to the

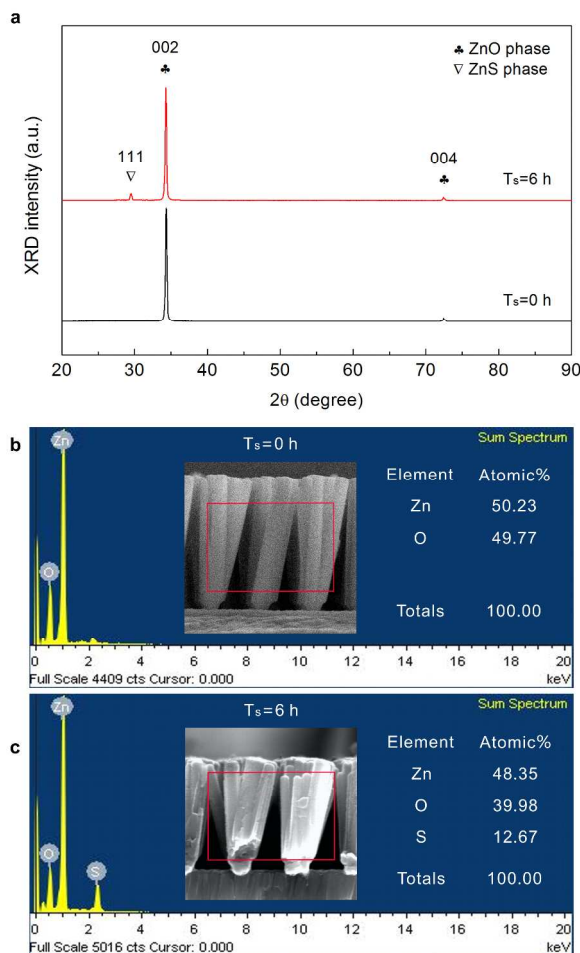


**Fig. 2** XRD patterns (a) and EDS spectra (b,c) of the patterned ZnO NWAs ( $T_s = 0$  h) and ZnO-ZnS core-shell NWAs ( $T_s = 6$  h) with line symmetry. Insets show the corresponding cross-sectional view SEM images, scanning areas and elemental atomic ratios of the NWAs.

one presented in previous works<sup>39,40</sup> and proves the existence of ZnS phase. Besides, the EDS spectrum demonstrates that the patterned ZnO NWAs are composed of only Zn and O elements (Fig. 2b). After sulfidation, Zn, O and S are the primary elements due to the fact that lots of O atoms were replaced by S atoms (Fig. 2c).<sup>38</sup> Moreover, the elemental atomic ratio of S is 12.67%, which is smaller than O. That's is because the ZnS shell is very thin ( $\sim 50$  nm),<sup>15</sup> and some ZnO core will be partially exposed if we want to obtain the cross-sectional view SEM image. In addition, the inserted cross-sectional view SEM images show that the NWAs have relatively small diameters at the root due to the confinement of PR templates,<sup>34</sup> and have uniform triangular space between two adjacent units, which will be conducive to sufficient dye absorption during the sensitization process.

To achieve patterned ZnO-ZnS core-shell NWAs with tunable arrangement and density, PR hole templates (Fig. S1b-d, ESI†) were also utilized. Based on PR line template, there are  $\sim 7.5 \times 10^4$  nanowires in each line unit, and the unit density is 2.0

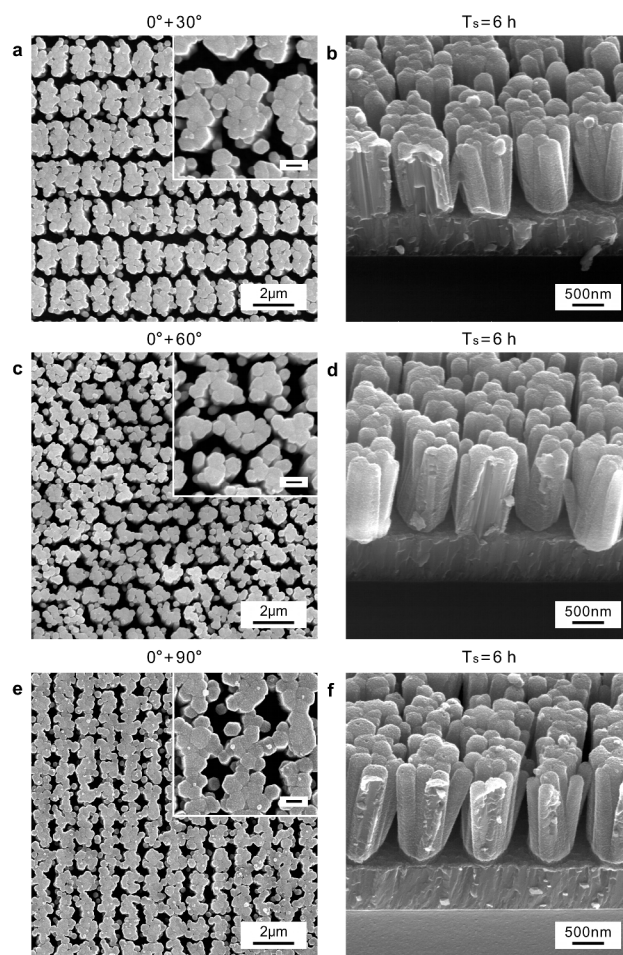


**Fig. 3** Top and  $45^\circ$  titled view SEM images of the patterned ZnO-ZnS core-shell NWAs with (a,b) long hexagonal, (c,d) hexagonal and (e,f) square symmetries, respectively. The sulfidation time  $T_s$  of each NWAs was 6 h. Insets present the corresponding magnified SEM images, scale bars are 300 nm.

$\times 10^4$   $\text{cm}^{-2}$  (Fig. 1d). In contrast, by using the PR hole templates with long hexagonal, hexagonal and square symmetries, the numbers of nanowires in each hole unit are adjusted from approximately 13, 7 to 10, and the unit densities are change from  $0.5 \times 10^8$ ,  $1.1 \times 10^8$  to  $1.0 \times 10^8$   $\text{cm}^{-2}$ , respectively (Fig. 3a,c,e). Obviously, the patterned NWAs with hexagonal symmetry have the minimum nanowires in each unit and the maximum unit density, and the patterned NWAs with line symmetry are just the opposite. An even larger unit density could be achieved by using shorter wavelength laser or larger incident angle.<sup>34,35</sup> Furthermore, all the patterned NWAs show a smooth ZnO core and a coarse ZnS shell (Fig. 3b,d,f), which is consistent with the SEM and TEM results reported in previous works.<sup>15,39,40</sup> Additionally, both the patterned NWAs and the substrates are covered with the ZnS shell, which will help to reduce the recombination of the electrons with either the dye or the electrolyte more effectively.<sup>14</sup>

As we mentioned, maximum light absorption on photoanode

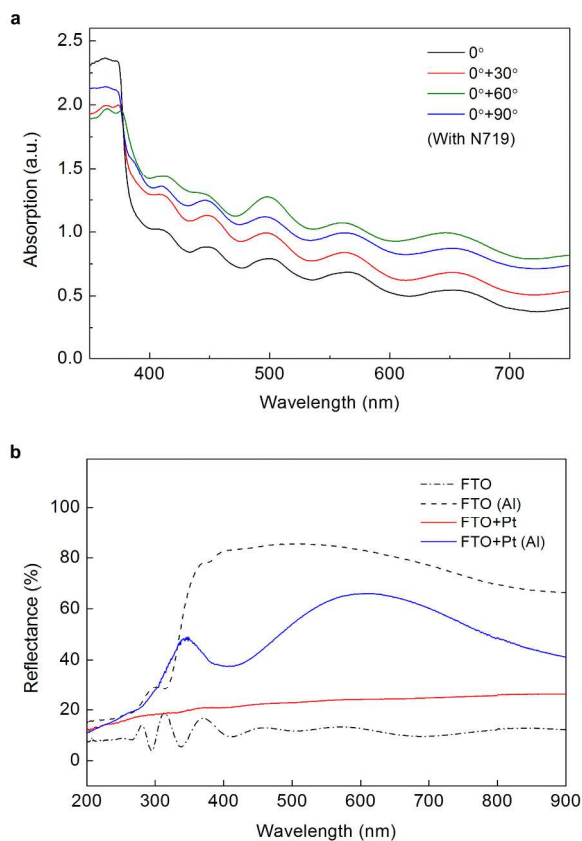


**Fig. 4** (a) UV-vis absorption spectra of the patterned ZnO-ZnS core-shell NWAs with four different symmetries. The NWAs were sensitized by N719 dye under the same conditions. (b) Reflectance spectra of the FTO glasses and FTO-Pt cathodes with or without Al reflecting layer.

and maximum light reflection on cathode are the key to achieve higher efficiency DSSCs. Therefore, the light absorption properties of the patterned ZnO-ZnS core-shell NWAs with four different symmetries were investigated after they were sensitized by N719 dye at the same conditions. Interestingly, the UV-vis absorption spectra show that all the patterned NWAs have a wide absorbance band in the visible region, and the NWAs with hexagonal symmetry demonstrate the highest absorption than the others (Fig. 4a). In general, ZnO-ZnS has low and smooth visible absorption due to its wide band gap property.<sup>11,13</sup> Hence, the enhanced absorption in visible region may attribute to the light scattering effect of the patterned NWAs,<sup>28</sup> and the wavy absorption may result from the light interference caused by the patterned NWAs with a fixed period of 1  $\mu\text{m}$ . What's more, the absorption trend in UV region is nearly opposite with the one in visible, and the NWAs with line and square symmetries show higher results due to their higher nanowire densities ( $1.5 \times 10^9$  and  $1.0 \times 10^9 \text{ cm}^{-2}$ ). Besides, it is clear that an absorption peak is centered around 505 nm, which is originating from the N719 dye molecules,<sup>14</sup> and the patterned NWAs in hexagonal symmetry present the highest value again. Generally, as the surface area of photoanode is enlarged, the

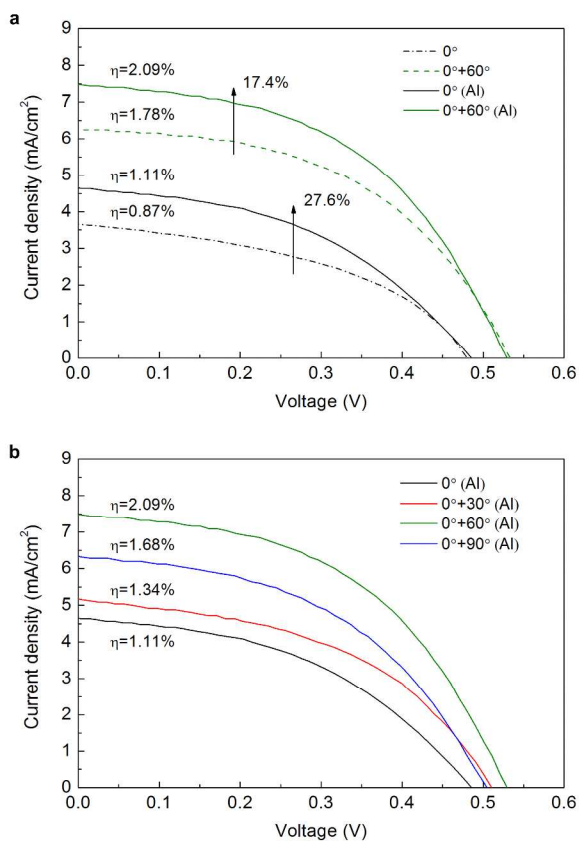


**Fig. 5** (a) J-V curves of the DSSCs based on patterned ZnO-ZnS core-shell NWAs photoanodes with line and hexagonal symmetries and FTO-Pt cathodes with or without Al reflecting layer. (b) J-V curves of the DSSCs based on the NWAs photoanodes with four different symmetries and FTO-Pt cathodes with Al reflecting layer.

amount of dye will be increased and more light can be harvested.<sup>15</sup> The NWAs with hexagonal symmetry have the minimum nanowires in each unit and maximum unit density, which are beneficial to the increase in surface area. Hence, the enhanced light harvesting of the patterned NWAs photoanode is attributed to not only the superior light scattering effect but also the enlarged surface area.

As the incident light can not be totally absorbed by the ZnO-ZnS core-shell NWAs photoanodes at once, in this study, FTO-Pt cathode with Al reflecting layer on the back side was employed to reflect the unabsorbed light back to the photoanodes and to realize double absorption. The reflectance spectra of the FTO-Pt cathodes with or without Al reflecting layer are presented in Fig. 4b. Before Pt deposition, FTO with Al reflecting layer has high reflectivity, showing a stark contrast to pure FTO, especially when the wavelength is longer than 350 nm. After Pt ( $\sim 20$  nm) was deposited, the reflectance of FTO is increased from  $\sim 10\%$  to  $\sim 20\%$ . Although the reflectance of FTO-Pt with Al reflecting layer is decreased, it is still much higher than FTO-Pt, which also can be seen

**Table 1** Comparison of photovoltaic properties of the DSSCs. Measurements were performed under 1 sun illumination (AM 1.5G, light intensity: 100 mW cm<sup>-2</sup>). The active areas were ~0.25 cm<sup>2</sup> for all of the cells and the data presented are average values obtained after testing 5 cells.

DSSC	Photoanode		Cathode	V <sub>oc</sub> (V)	J <sub>sc</sub> (mA cm <sup>-2</sup> )	FF	η (%)
	Symmetry	Unit density (cm <sup>-2</sup> )					
1	Line	2.0×10 <sup>4</sup>	FTO+Pt	0.49	3.66	0.44	0.87
2	Hexagonal	1.1×10 <sup>8</sup>		0.53	6.24	0.49	1.78
3	Line	2.0×10 <sup>4</sup>		0.49	4.64	0.44	1.11
4	Long hexagonal	0.5×10 <sup>8</sup>	FTO+Pt (Al)	0.51	5.15	0.46	1.34
5	Hexagonal	1.1×10 <sup>8</sup>		0.52	7.44	0.48	2.09
6	Square	1.0×10 <sup>8</sup>		0.51	6.32	0.47	1.68

obviously from the optical images (Fig. S2a, ESI†). Therefore, the DSSCs assembled with patterned ZnO-ZnS core-shell NWAs photoanode and FTO-Pt cathode with Al reflecting layer can collect the incident light in three ways, including direct absorption by dye, and second absorptions by dye through reflecting the unabsorbed light by Pt and Al layers (Fig. S2b, ESI†). In this way, the incident light can be collected more efficiently, which will be helpful to the improvement of J<sub>sc</sub>.<sup>27,28</sup> Thus the J<sub>sc</sub> will be increased by enhanced light harvesting on both patterned NWAs photoanode and FTO-Pt cathode. Noted that the J<sub>sc</sub> can further be enhanced by the ZnS shell, because it can reduce the defect sites on the ZnO surface and form a higher band gap than ZnO, which suppress the recombination of injected electrons with either the N719 dye or the redox electrolyte (Fig. S2c, ESI†).<sup>13-15</sup>

The photoelectric characteristics of the DSSCs, such as open circuit voltage (V<sub>oc</sub>), short circuit current density (J<sub>sc</sub>), fill factor (FF) and power conversion efficiency (η), are summarized in Table 1. Before using the Al reflecting layer, the DSSCs based on patterned ZnO-ZnS core-shell NWAs photoanodes with line symmetry exhibited a V<sub>oc</sub> of 0.49 V, a J<sub>sc</sub> of 3.66 mA cm<sup>-2</sup>, a FF of 0.44 and a η of 0.87%, and with hexagonal symmetry demonstrated a V<sub>oc</sub> of 0.53 V, a J<sub>sc</sub> of 6.24 mA cm<sup>-2</sup>, a FF of 0.49 and a η of 1.78% (Fig. 5a). After using the Al reflecting layer, the cells show no significant changes in V<sub>oc</sub> and FF, but have increased J<sub>sc</sub> thus higher η of 1.11% and 2.09%, respectively. Therefore, the Al reflecting layer is proved to be helpful to the double absorption of incident light and efficiency improvement of the DSSCs. In addition, the improvement of η for hexagonal symmetry is 17.4%, but 27.6% for line symmetry, due to less light absorption on photoanode at once will lead to more light absorption for the second time.

In general, the number of photo-generated carriers in DSSCs is a most important factor to determine the J<sub>sc</sub> and η, and can be affected by the light-harvesting capability of the photoanodes with different configurations.<sup>28</sup> Hence, a comparison was made among the DSSCs assembled with the four different NWAs photoanodes and FTO-Pt cathodes with the Al reflecting layer (Fig. 5b). Obviously, the hexagonal symmetry photoanode results in the highest J<sub>sc</sub> and η of 7.44 mA cm<sup>-2</sup> and 2.09%, which are approximately 60% and 88% enhancement to the one with line symmetry. The results are consistent with the UV-vis absorption spectra shown in Fig. 4a, and what's more, indicate that the arrangement and density of patterned ZnO-ZnS core-

shell NWAs have remarkable influence on the performance of the DSSCs. In this case, patterned ZnO-ZnS core-shell NWAs with minimum nanowires in each unit, maximum unit density and hexagonal symmetry are the best option for realizing efficient DSSCs.

## Conclusion

In summary, we have developed an effective method to fabricate large-scale patterned ZnO-ZnS core-shell NWAs and boost the light-harvesting efficiency of the DSSCs. The arrangement and density of the NWAs have remarkable influence on the performance of the cells. The DSSCs, based on the NWAs photoanode with hexagonal symmetry and FTO-Pt cathode with Al reflecting layer, achieve the highest efficiency of 2.09%, which is improved by 140% compared to the reference cells with line symmetry and without reflecting layer. The improvement can be explained by the excellent light-scattering effect and enlarged surface area of the patterned NWAs, as well as the remarkable double absorption caused by the Al reflecting layer. Besides, the ZnO core provides direct and quick pathway for electron transfer, and the ZnS shell reduces the recombination of injected electrons with either the dye or the electrolyte. Although we focus on ZnO-ZnS as a model here, this method is highly generic for various semiconductors, including inorganic oxides, quantum dots and organic materials,<sup>41,42</sup> and can be applied to many other nanodevices and nanosystems in the future.

## Acknowledgements

This work was supported by the National Major Research Program of China (2013CB932602), the Major Project of International Cooperation and Exchanges (2012DFA50990), the Program of Introducing Talents of Discipline to Universities, NSFC (51232001, 51172022, 51372023), the Fundamental Research Funds for the Central Universities, and Program for Changjiang Scholars and Innovative Research Team in University.

## Notes and references

<sup>a</sup> State Key Laboratory for Advanced Metals and Materials, School of Materials Science and Engineering, University of Science and Technology Beijing, Beijing 100083, China. Tel: +86-10-62334725; E-mail: yuezhang@ustb.edu.cn

<sup>b</sup> Key Laboratory of New Energy Materials and Technologies, University of Science and Technology Beijing, Beijing 100083, China. Tel: +86-10-62334725; E-mail: yuezhang@ustb.edu.cn

† Electronic Supplementary Information (ESI) available: SEM images of the PR templates obtained by using 2BLIL with four exposure modes, optical images of the FTO-Pt cathodes with or without Al reflecting layer, schematic illustration of the presented DSSCs and light transport path, and energy level diagram for the ZnO-ZnS core-shell NWAs with N719 dye in electrolyte. See DOI: 10.1039/b000000x/

‡ These authors contributed equally to this work.

- 1 M. Grätzel, *J. Photoch. Photobio. C*, 2003, **4**, 145.
- 2 V. Thavasi, V. Renugopalakrishnan, R. Jose and S. Ramakrishna, *Mater. Sci. Eng. R*, 2009, **63**, 81.
- 3 J. Bouclé and J. Ackermann, *Polym. Int.*, 2012, **61**, 355.
- 4 M. Yu, Y. Z. Long, B. Sun and Z. Fan, *Nanoscale*, 2012, **4**, 2783.
- 5 B. O'Regan and M. Grätzel, *Nature*, 1991, **353**, 737.
- 6 A. Yella, H. W. Lee, H. N. Tsao, C. Yi, A. K. Chandiran, M. K. Nazeeruddin, E. W. Diau, C. Y. Yeh, S. M. Zakeeruddin and M. Grätzel, *Science*, 2011, **334**, 629.
- 7 T. Chen, W. Hu, J. Song, G. H. Guai and C. M. Li, *Adv. Funct. Mater.*, 2012, **22**, 5245.
- 8 Y. Bai, H. Yu, Z. Li, R. Amal, G. Q. Lu and L. Wang, *Adv. Mater.*, 2012, **24**, 5850.
- 9 Y.-Z. Zheng, X. Tao, Q. Hou, D.-T. Wang, W.-L. Zhou and J.-F. Chen, *Chem. Mater.*, 2011, **23**, 3.
- 10 M. Law, L. E. Greene, J. C. Johnson, R. Saykally and P. Yang, *Nat. Mater.*, 2005, **4**, 455.
- 11 Q. Zhang, C. S. Dandeneau, X. Zhou and G. Cao, *Adv. Mater.*, 2009, **21**, 4087.
- 12 V. O. Williams, N. C. Jeong, C. Prasittichai, O. K. Farha, M. J. Pellin and J. T. Hupp, *ACS nano*, 2012, **6**, 6185.
- 13 J. Chung, J. Myoung, J. Oh and S. Lim, *J. Phys. Chem. C*, 2010, **114**, 21360.
- 14 X.-L. Yu, J.-G. Song, Y.-S. Fu, Y. Xie, X. Song, J. Sun and X.-W. Du, *J. Phys. Chem. C*, 2010, **114**, 2380.
- 15 L. Liu, Y. Chen, T. Guo, Y. Zhu, Y. Su, C. Jia, M. Wei and Y. Cheng, *ACS Appl. Mater. Interfaces*, 2012, **4**, 17.
- 16 Y. Sun, J. Yang, L. Yang, J. Cao, M. Gao, Z. Zhang, Z. Wang and H. Song, *J. Solid State Chem.*, 2013, **200**, 258.
- 17 S. Saha, S. Sarkar, S. Pal and P. Sarkar, *J. Phys. Chem. C*, 2013, **117**, 15890.
- 18 S. H. Ko, D. Lee, H. W. Kang, K. H. Nam, J. Y. Yeo, S. J. Hong, C. P. Grigoropoulos and H. J. Sung, *Nano Lett.*, 2011, **11**, 666.
- 19 C. Xu, J. Wu, U. V. Desai and D. Gao, *Nano Lett.*, 2012, **12**, 2420.
- 20 M. McCune, W. Zhang and Y. Deng, *Nano Lett.*, 2012, **12**, 3656.
- 21 S. Nishimura, N. Abrams, B. A. Lewis, L. I. Halaoui, T. E. Mallouk, K. D. Benkstein, J. van de Lagemaat and A. J. Frank, *J. Am. Chem. Soc.*, 2003, **125**, 6306.
- 22 S. Guldin, S. Huttner, M. Kolle, M. E. Welland, P. Müller-Buschbaum, R. H. Friend, U. Steiner and N. Tetreault, *Nano Lett.*, 2010, **10**, 2303.
- 23 V. E. Ferry, J. N. Munday and H. A. Atwater, *Adv. Mater.*, 2010, **22**, 4794.
- 24 H. A. Atwater and A. Polman, *Nat. Mater.*, 2010, **9**, 205.
- 25 M. D. Brown, T. Suteewong, R. S. Kumar, V. D'Innocenzo, A. Petrozza, M. M. Lee, U. Wiesner and H. J. Snaith, *Nano Lett.*, 2011, **11**, 438.
- 26 H. Tan, R. Santbergen, A. H. Smets and M. Zeman, *Nano Lett.*, 2012, **12**, 4070.
- 27 J. Kim, J. K. Koh, B. Kim, J. H. Kim and E. Kim, *Angew. Chem. Int. Ed.*, 2012, **51**, 6864.
- 28 K. S. Kim, H. Song, S. H. Nam, S. M. Kim, H. Jeong, W. B. Kim and G. Y. Jung, *Adv. Mater.*, 2012, **24**, 792.
- 29 E. Garnett and P. Yang, *Nano Lett.*, 2010, **10**, 1082.
- 30 V. E. Ferry, M. A. Verschuuren, M. C. Lare, R. E. Schropp, H. A. Atwater and A. Polman, *Nano Lett.*, 2011, **11**, 4239.
- 31 Q. Lin, B. Hua, S. F. Leung, X. Duan and Z. Fan, *ACS nano*, 2013, **7**, 2725.
- 32 Y. Yang, K. Mielczarek, M. Aryal, A. Zakhidov and W. Hu, *ACS nano*, 2012, **6**, 2877.
- 33 D. Chen, W. Zhao and T. P. Russell, *ACS nano*, 2012, **6**, 1479.
- 34 X. Chen, X. Yan, Z. Bai, P. Lin, Y. Shen, X. Zheng, Y. Feng and Y. Zhang, *CrystEngComm*, 2013, **15**, 8022.
- 35 X. Chen, X. Yan, Z. Bai, Y. Shen, Z. Wang, X. Dong, X. Duan and Y. Zhang, *CrystEngComm*, 2013, **15**, 8416.
- 36 D. Xia, Z. Ku, S. C. Lee and S. R. Brueck, *Adv. Mater.*, 2011, **23**, 147.
- 37 S. Xu, Y. Wei, M. Kirkham, J. Liu, W. Mai, D. Davidovic, R. L. Snyder and Z. L. Wang, *J. Am. Chem. Soc.*, 2008, **130**, 14958.
- 38 W. H. Nam, Y. S. Lim, W.-S. Seo, H. K. Cho and J. Y. Lee, *J. Nanopart. Res.*, 2011, **13**, 5825.
- 39 X. M. Shuai and W. Z. Shen, *J. Phys. Chem. C*, 2011, **115**, 6415.
- 40 Y. Hu, H. Qian, Y. Liu, G. Du, F. Zhang, L. Wang and X. Hu, *CrystEngComm*, 2011, **13**, 3438.
- 41 Y. Yang, W. Guo, K. C. Pradel, G. Zhu, Y. Zhou, Y. Zhang, Y. Hu, L. Lin and Z. L. Wang, *Nano Lett.*, 2012, **12**, 2833.
- 42 Y. Yang, H. Zhang, G. Zhu, S. Lee, Z. Lin and Z. L. Wang, *ACS nano*, 2013, **7**, 785.